Journal of Solid Mechanics Vol. 3, No. 1 (2011) pp. 9-18

Magneto-Thermo-Elastic Behavior of Cylinder Reinforced with FG SWCNTs Under Transient Thermal Field

A. Ghorbanpour Arani [1,2*], M.R. Mozdianfard [3], V. Sadooghi[1], M. Mohammadimehr[1], R. Kolahchi[1]

[1]*Department of Mechanical Engineering, Faculty of Engineering, University of Kashan, Kashan, Iran*
[2]*Institute of Nano science & Nanotechnology, University of Kashan, Kashan, Iran*
[3]*Department of Chemical Engineering, Faculty of Engineering, University of Kashan, Kashan, Iran*

Received 15 December 2010; accepted 11 February 2011

ABSTRACT

In this article, magneto-thermo-elastic stresses and perturbation of magnetic field vector are analyzed for a thick-walled cylinder made from polystyrene, reinforced with functionally graded (FG) single-walled carbon nanotubes (SWCNTs) in radial direction, while subjected to an axial and uniform magnetic field as well as a transient thermal field. Generalized plane strain state is considered in this study. The SWCNTs are assumed aligned, straight with infinite length. Two types of variations in the volume fraction of SWCNTs were considered in the structure of the FG cylinder along the radius from inner to outer surface, namely: functionally graded increasing (FG Inc) and functionally graded decreasing (FG Dec) which are then compared with uniformly distributed (UD) layouts. The constitutive equations of this type of reinforced polymeric cylinder are derived by Mori-Tanaka method. Following the introduction of a second order partial differential equation derived from the equations of motion and stress-strain relationships and solving by a semi-analytical method, distribution of stresses and perturbation of magnetic field vector are obtained. Results indicate that maximum radial and circumferential stresses occur in FG Inc and FG Dec layouts, respectively. Maximum perturbation of magnetic field vector is not affected by UD layout.

Keywords: Magneto-thermo-elastic stresses; Perturbation of magnetic field vector; FG SWCNTs; Cylinder; Transient thermal field.

1 INTRODUCTION

DEVELOPMENT of carbon nanotunbes (CNTs) reinforced composites in recent decades, have improved composite properties, such as tensile strength, stiffness, thermal conductivity, elastic modulus and magnetic characteristics [1-4]. Fidelus et al. [5] studied the thermo-mechanical properties of epoxy-based nano composites based on low weight fractions of randomly oriented single and multi-walled carbon nanotubes (SWCNTs and MWCNTs). Using only minute nanotube weight fractions, they obtained a particularly significant enhancement of the tensile impact toughness for specific nano composites and observed no significant change in the glass transition temperature of SWCNT/epoxy nano composites, compared to that of the epoxy matrix. Also, they found that the elastic modulus of the SWCNT based nano composites were slightly higher than those predicted by the Krenchel model for short-fiber composites with random orientation. Ghorbanpour Arani [6] considered the buckling analysis of laminated composite plates reinforced by SWCNTs using an analytical approach and finite element method (FEM) based on the classical laminated plate theory (CLPT), third-order shear deformation theory and Mori-Tanaka method.

* Corresponding author. Tel.: +98 913 162 6594; fax: +98 361 551 3011.
E-mail address: *aghorban@kashanu.ac.ir* (A. Ghorbanpour Arani).

Functionally graded materials (FGMs) are a new generation of composites in which the micro structural details are spatially varied through non-uniform distribution of the reinforcement phase in order to improve properties such as linear and nonlinear bending behaviors, and interfacial bonding strength. Shen [7] studied these for the plates at various thermal environments; while Ke et al. [8] examined nonlinear free-vibration of FGM CNT reinforced composites for beams. Shen and Zhang [9] presented thermal buckling and post buckling behavior for FGM plates reinforced by SWCNTs subjected to in-plane temperature variation. They assumed material properties of SWCNTs are temperature-dependent and evaluated them from molecular dynamics simulations. Regarding the estimation of the material properties of the reinforced composite structure, (FG-CNTRCs) they used a micromechanical model for grading in thickness direction. Based on the multi-scale approach, numerical results are presented for perfect and imperfect geometrically mid-plane symmetric FG-CNTRC plates and uniformly distributed CNTRC plates for different nanotube volume fractions.

To date, no investigation on Magneto-thermo-elastic behavior of a polymeric cylinder reinforced with FG SWCNTs using Mori-Tanaka method has been reported in the literatures. In this article, Magneto-thermo-elastic stresses and perturbation of magnetic field vector for a thick-walled cylinder made from polystyrene reinforced with SWCNTs for various CNTs layouts under uniform magnetic and transient thermal fields are analyzed. Distribution of transient stresses and perturbation of magnetic field vectors are obtained and studied using the semi-analytical method.

2 BASIC FORMULATION

To introduce the basic analytical relationships, first stress-strain relations are obtained for the thick-walled nanocomposite cylinder based on conservation of mass law. For this, consider a thick-walled polystyrene cylinder with cylindrical coordinate system (r,θ,z) reinforced by SWCNTs as shown in Fig.1. The inner and outer radii of the cylinder denote r_i and r_o, respectively. Using, Mori-Tanaka method, the effective material properties of the polystyrene reinforced by SWCNTs are determined. The volume fraction of the constituent for both the reinforced CNT and the matrix are c_r and c_m, respectively, then [7]:

$$c_r + c_m = 1 \tag{1}$$

As can be seen from Fig.1, when the volume fraction of SWCNTs is uniformly distributed (UD) from inner to outer surface, c_r is defined as follows [7]:

$$c_r = V_{CN}^{*} \tag{2}$$

where $V_{CN}^{*} = \dfrac{w_{CNT}}{w_{CNT} + (\rho_{CNT}/\rho_m) - (\rho_{CNT}/\rho_m) w_{CNT}}$ and $w_{CNT} = 0.13$ is the mass fraction of the SWCNTs, ρ_m and ρ_{CNT} are densities of matrix and carbon nanotubes, respectively, and $V_{CN}^{*} = 0.11$ is the specific volume fraction of carbon nanotube. In this study, two types of variations (or layouts) in the volume fraction of SWCNTs are considered in the structure of the FG cylinder along the radius from inner to outer surface, namely: incrementally decreasing (FG Dec) and incrementally increasing (FG Inc) (see Fig. 1). The former refers to the structure in which the volume fraction of the SWCNTs is reduced from inner to outer surface, while for the latter, this is increased. c_r for both FG Dec and FG Inc are as explained below in Eqs .(3-4) , respectively.

$$c_r = \left(1 + 2\frac{1-\zeta}{1-R}\right) V_{CN}^{*} \tag{3}$$

$$c_r = \left(1 + 2\frac{1-\zeta}{1-R}\right) V_{CN}^{*} \tag{4}$$

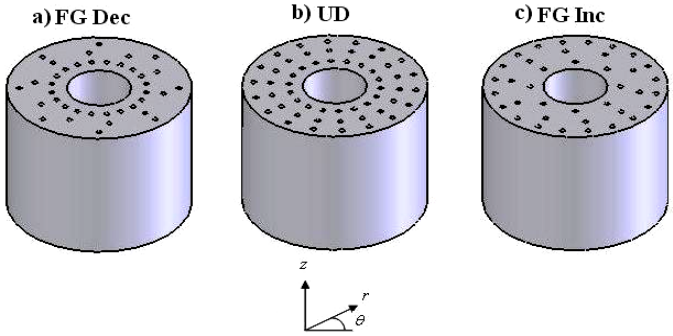

Fig. 1
Variations in the volume fraction of SWCNTs in the axial direction throughout the thickness of the thick-walled cylinder considered: a) Functionally graded increase (FG Inc), b) Uniformly distributed (UD) and c) Functionally graded decrease (FG Dec).

where ζ and R are the dimensionless radius and ratio of the inner to outer radius of the cylinder (aspect ratios), respectively, i.e.

$$\zeta = \frac{r}{r_o}, \qquad R = \frac{r_i}{r_o} \tag{5}$$

2.1 Thermal analysis

The general equations of motion and kinematic relations for a thick-walled cylinder could be written as [10]:

$$\begin{aligned}
&\frac{\partial \sigma_{rr}}{\partial r} + \frac{1}{r}\frac{\partial \sigma_{r\theta}}{\partial \theta} + \frac{\partial \sigma_{rz}}{\partial z} + \frac{\sigma_{rr} - \sigma_{\theta\theta}}{r} + F_r = \rho \frac{\partial^2 u_r}{\partial t^2} \\
&\frac{\partial \sigma_{\theta r}}{\partial r} + \frac{1}{r}\frac{\partial \sigma_{\theta\theta}}{\partial \theta} + \frac{\partial \sigma_{\theta z}}{\partial z} + \frac{2\sigma_{\theta r}}{r} + F_\theta = \rho \frac{\partial^2 u_\theta}{\partial t^2} \\
&\frac{\partial \sigma_{zr}}{\partial r} + \frac{1}{r}\frac{\partial \sigma_{z\theta}}{\partial \theta} + \frac{\partial \sigma_{zz}}{\partial z} + \frac{\sigma_{zr}}{r} + F_z = \rho \frac{\partial^2 u_z}{\partial t^2}
\end{aligned} \tag{6}$$

$$\begin{aligned}
&\varepsilon_{rr} = \frac{\partial u_r}{\partial r}, \qquad \varepsilon_{\theta\theta} = \frac{1}{r}\frac{\partial u_\theta}{\partial \theta} + \frac{u_r}{r}, \qquad \varepsilon_{zz} = \frac{\partial u_z}{\partial z}, \\
&\varepsilon_{r\theta} = \frac{1}{2}\left(\frac{\partial u_\theta}{\partial r} + \frac{1}{r}\frac{\partial u_r}{\partial \theta} - \frac{u_\theta}{r}\right), \qquad \varepsilon_{\theta z} = \frac{1}{2}\left(\frac{\partial u_\theta}{\partial z} + \frac{1}{r}\frac{\partial u_z}{\partial \theta}\right), \qquad \varepsilon_{rz} = \frac{1}{2}\left(\frac{\partial u_z}{\partial r} + \frac{\partial u_r}{\partial z}\right)
\end{aligned} \tag{7}$$

Then the nano composite cylinder is subjected to a thermal field, thermal strains are created in three directions in the stress-strain relations based on Mori-Tanaka method as follows [11]:

$$\begin{Bmatrix} \sigma_r \\ \sigma_z \\ \sigma_\theta \\ \sigma_{\theta z} \\ \sigma_{zr} \\ \sigma_{r\theta} \end{Bmatrix} = \begin{bmatrix} C_{11} & C_{12} & C_{13} & 0 & 0 & 0 \\ C_{21} & C_{22} & C_{23} & 0 & 0 & 0 \\ C_{31} & C_{32} & C_{33} & 0 & 0 & 0 \\ 0 & 0 & 0 & C_{44} & 0 & 0 \\ 0 & 0 & 0 & 0 & C_{55} & 0 \\ 0 & 0 & 0 & 0 & 0 & C_{66} \end{bmatrix} \begin{Bmatrix} \varepsilon_r - \lambda_r T \\ \varepsilon_z - \lambda_z T \\ \varepsilon_\theta - \lambda_\theta T \\ 2\gamma_{\theta z} \\ 2\gamma_{zr} \\ 2\gamma_{r\theta} \end{Bmatrix} \tag{8}$$

where C_{ij} are composed of Hill's elastic moduli [11]. $\lambda_i\,(i=r,z,\theta)$ is the thermal modulus, and T denotes temperature. In Eq. (8), elastic moduli and thermal expansion coefficients are related as follows [10]:

$$\begin{aligned}\lambda_r &= C_{11}\alpha_r + C_{12}\alpha_z + C_{13}\alpha_\theta \\ \lambda_z &= C_{21}\alpha_r + C_{22}\alpha_z + C_{23}\alpha_\theta \\ \lambda_\theta &= C_{31}\alpha_r + C_{32}\alpha_z + C_{33}\alpha_\theta\end{aligned} \tag{9}$$

Based on Mori-Tanaka method, nano composite characteristics are assumed to be transversely isotropic which can only be applied where SWCNTs are uniformly distributed. This is because the nano composite characteristics are orthotropic for FG materials. Despite this, assuming the structure is almost uniform and c_r changes slightly and linearly in such a way that properties do not vary significantly in radial and circumferential directions, one might employ the introduced stiffness matrix in Eq. (8) for FG materials. The thermal expansion coefficients of nano composite in r,z and θ directions may be written as [7]:

$$\alpha_r = (1+\nu_z^{CN})c_r\alpha_r^{CN} + (1+\nu_m)c_m\alpha^m - \nu_\zeta \times \alpha_z \tag{10a}$$

$$\alpha_z = c_r\alpha_z^{CN} + c_m\alpha^m \tag{10b}$$

$$\alpha_r = \alpha_\theta \tag{10c}$$

$$\nu_\zeta = c_r\nu_z^{CN} + c_m\nu_m \tag{10d}$$

where $\alpha_r^{CN}, \alpha_z^{CN}$ are thermal expansion coefficients of SWCNTs in longitudinal and radial directions, respectively, and α^m is the thermal expansion coefficient of the matrix assumed to be $\alpha^m = 7\times10^{-5}(\mathrm{K}^{-1})$ [12]. However, $\alpha_r^{CN}, \alpha_z^{CN}$ are not expected to vary significantly for the temperature range of 300K<T<700K considered in this work. Hence, their average values are taken at 500K from the data used by [7]. Also, in the above equations, ν_z^{CN}, ν_m are Poisson's ratios SWCNTs and matrix assumed to be $\nu_z^{CN} = 0.175,\ \nu_m = 0.3$ [7, 11]. For practical purposes, stress, strain and thermal module can be rewritten in dimensionless form as follows:

$$\begin{aligned}&\theta = \frac{T}{T_0}, \qquad \varepsilon_\theta = \alpha_r T_0 \frac{u_0}{\zeta}, \qquad \varepsilon_r = \alpha_r T_0 \frac{\partial u_0}{\partial \zeta}, \qquad u_0 = \frac{u}{\alpha_r T_0 b}, \qquad \tau = \frac{1}{r_o}\sqrt{\frac{C_{11}}{\rho_m}}t \\ &\Lambda_i = \frac{\lambda_i}{C_{11}\alpha_r} \quad (i=r,z,\theta), \qquad \sigma_i = \frac{\sigma_{ii}}{\alpha_r T_0 C_{11}}, \qquad (i=r,z,\theta)\end{aligned} \tag{11}$$

The general form of the governing equation of heat conduction in cylindrical coordinates can be written as [13]:

$$k\left(\frac{\partial^2 T}{\partial r^2} + \frac{1}{r}\frac{\partial T}{\partial r} + \frac{1}{r^2}\frac{\partial^2 T}{\partial \vartheta^2} + \frac{\partial^2 T}{\partial z^2}\right) + R = \rho c_p \frac{\partial T}{\partial t} \tag{12}$$

where R, c_p and k are nano composite rate of heat generation, specific thermal capacity and conductivity respectively. Assuming long enough cylinder, no internal heat generation, transient thermal field and axisymmetrical temperature distribution (i.e. $\frac{\partial^2 T}{\partial \vartheta^2} = 0$, $\frac{\partial^2 T}{\partial z^2} = 0$), the heat transfer equation based on the boundary condition is simplified to [13]:

$$r_o c_v \frac{\partial \theta}{\partial \tau} = K_e\left(\frac{\partial^2 \theta}{\partial \zeta^2} + \frac{1}{\zeta}\frac{\partial \theta}{\partial \zeta}\right) \tag{13}$$

where

$$c_v = \sqrt{\frac{C_{11}}{\rho_m}}, \qquad K_e = \frac{k}{\rho c_p}$$

Thermal boundary conditions are considered as;

$$T(r_i,t) = 300\text{K}, \qquad T(r_o,t) = 500\text{K}, \qquad T(r_i,0) = 300\text{K} \tag{14}$$

It is important to define the effect of reinforcement and matrix in Eq. (13). The conductivity, density, and specific heat coefficients of nano composite defined as [8, 14, 15]:

$$\frac{k}{k_m} = \frac{3 + c_r k_{CNT} / k_m}{3 - 2c_r} \tag{15}$$

$$\rho = \rho_{CNT}\, c_r + \rho_m\, c_m \tag{16}$$

$$c_p = 60 + 999\theta + 1200 c_r \tag{17}$$

The conductivity for CNTs can be expressed as [16]:

$$k_{CNT} = -148.5\ \theta + 595.26 \tag{18}$$

2.2 Magnto-thermo-elastic analysis

Considered a thick-walled polymeric cylinder reinforced by SWNTs with internal radius r_i and external radius r_o placed in a uniform magnetic field $\overrightarrow{H}(0,0,H_z)$. For the following conditions, that is FG hollow cylinder subjected to a rapid temperature change $T(r,t)$, uniform magnetic permeability μ at the outer surface of the FG cylinder and the surrounding medium, non-ferromagnetic and non-ferroelectric medium, and ignoring displacement electric currents involved, the governing electrodynamics' Maxwell equations for a perfectly conducting elastic body can be written as [17]:

$$\begin{aligned} &\overline{J} = curl\,\overline{h}, \qquad div\,\overline{h} = 0, \\ &-\mu\frac{\partial \overline{h}}{\partial t} = curl\,\overline{h}, \qquad \overline{e} = -\mu\left(\frac{\partial \overline{U}}{\partial t} \times \overline{\mathrm{H}}\right), \end{aligned} \tag{19}$$

Applying a primary magnetic field vector $\overrightarrow{H}(0,0,H_z)$ to Eq. (22) yields

$$\begin{aligned} &\overline{U} = \overline{U}\left(u\left(r,t\right),0,0\right), \qquad \overline{\mathrm{H}} = \overline{\mathrm{H}}\left(0,0,\mathrm{H}_z\right), \qquad \overline{e} = \mu\left(0,-\mathrm{H}_z\frac{\partial u}{\partial t},0\right) \\ &\overline{h} = \mathrm{Curl}\ (\overline{U}\times\overline{\mathrm{H}}) = \left(0,0,-\mathrm{H}_Z\left(\frac{1}{r}\frac{\partial(ru)}{\partial r}\right)\right) = \left(0,0,-\mathrm{H}_z\left(\frac{\partial u}{\partial r}+\frac{u}{r}\right)\right) \\ &\overline{J} = \left(0,\frac{\partial h_z}{\partial r},0\right), \qquad \overline{h} = \left(0,0,h_z\right), \qquad h_z = -\mathrm{H}_z\left(\frac{\partial u}{\partial r}+\frac{u}{r}\right) \end{aligned} \tag{20}$$

where $\overline{J}$, $\overline{h}$, $\overline{e}$, and $\overline{U}$ are the electric current density vector, the perturbation of magnetic field vector, the perturbation of electric field vector, and the displacement vector, respectively. Considering Eq. (6) and (20), the magneto-thermo-elastic dynamic equation in the absence of body force, for a hollow cylinder may be written as:

$$\frac{\partial \sigma_r}{\partial r}+\frac{\sigma_r-\sigma_\theta}{r}+f_z=\rho\frac{\partial^2 u_0}{\partial t^2} \tag{21}$$

where f_z is Lorentz's force [17], defined as:

$$f_z=\mu(\bar{J}\times\bar{\mathrm{H}})=\mu \mathrm{H}_z^2\frac{\partial}{\partial r}\left(\frac{\partial u}{\partial r}+\frac{u}{r}\right) \tag{22}$$

μ is the magnetic permeability of nano composite that decomposed to magnetic permeability of matrix and reinforcement. It is assumed that magnetic permeability of matrix equals the magnetic permeability of the surrounding medium. ($\mu_m=4\pi\times10^{-7}$ and $\mu_{CN}=0.25$) [18]:

$$\mu=\mu_{CN}\,c_r+\mu_m\,c_m \tag{23}$$

The generalized plane strain state ($\varepsilon_z=0.01$), $u(\theta)=0$, and $u_r=u(r,t)$ are considered in formulation and using Eqs. (7), (8) and (21), the following second order partial differential equation is obtained:

$$\left(1+\frac{\mu H_z^{\,2}}{\alpha_r T_0 C_{11}}\right)\left(u_0^{\,//}+\frac{u_0^{\,/}}{\zeta}-\frac{u_0}{\zeta^2}\right)-\left(\frac{\partial \Lambda_r}{\partial \zeta}\theta+\Lambda_r\frac{\partial \theta}{\partial \zeta}\right)=\rho\frac{\partial^2 u_0}{\partial \tau^2} \tag{24}$$

The boundary conditions are written as follows:

$$\begin{aligned} &\sigma_r(R)=-2 && u_0(\zeta,0)=0\\ &\sigma_r(1)=0 && u^{\bullet}_{\,0}(\zeta,0)=0 \end{aligned} \tag{25}$$

The semi-analytical solution to this equation is provided by [19].

3 NUMERICAL RESULTS AND DISCUSSION

In this section, diagrams corresponding to distribution stresses and perturbation of magnetic field vector are discussed. Fig.2 shows distribution of dimensionless radial stress (σ_r) versus dimensionless time (τ) for various layout and dimensionless radius ($\zeta=0.4,\ 0.6,\ 0.8$ and 1) and indicates that the boundary conditions at the inner surface ($\sigma_r(R)=-2$) and at the outer surface ($\sigma_r(1)=0$) is satisfied. The obtained results show that stress amplitude decreases for various layouts with increase in dimensionless time and radius (ζ and τ). Maximum stress value takes place for FG Inc layout. It should be noted that, dimensionless radial stress stabilizes earlier in isotropic condition (Iso) compare to others. σ_r at steady state increases from inner to middle surface when ζ increases from 0.4 to 0.6 while, it decreases from middle to outer surface for ζ higher than 0.6. It is also clear from Fig.2 that radial stress appears to be tensional except for near the inner surfaces.

Fig.3 depicts distribution of dimensionless circumferential stress (σ_θ) versus dimensionless time (τ) for various layouts, behaving similar to radial stress. Dimensionless circumferential stress amplitude decreases with increasing ζ and τ values for different layouts, so that maximum stress at near the inner surface is about four times that at the outer surface of the cylinder. This might be due to collision and accumulation of the waves raised at inner surface of the cylinder with each other leading to very large wave peaks. Maximum stress value is related to FG Dec layout. The dimensionless circumferential stress stabilizes earlier again for (Iso) conditions compared with others. The circumferential stress, however, appears to remain tensional in nature irrespective of the radius of cylinder.

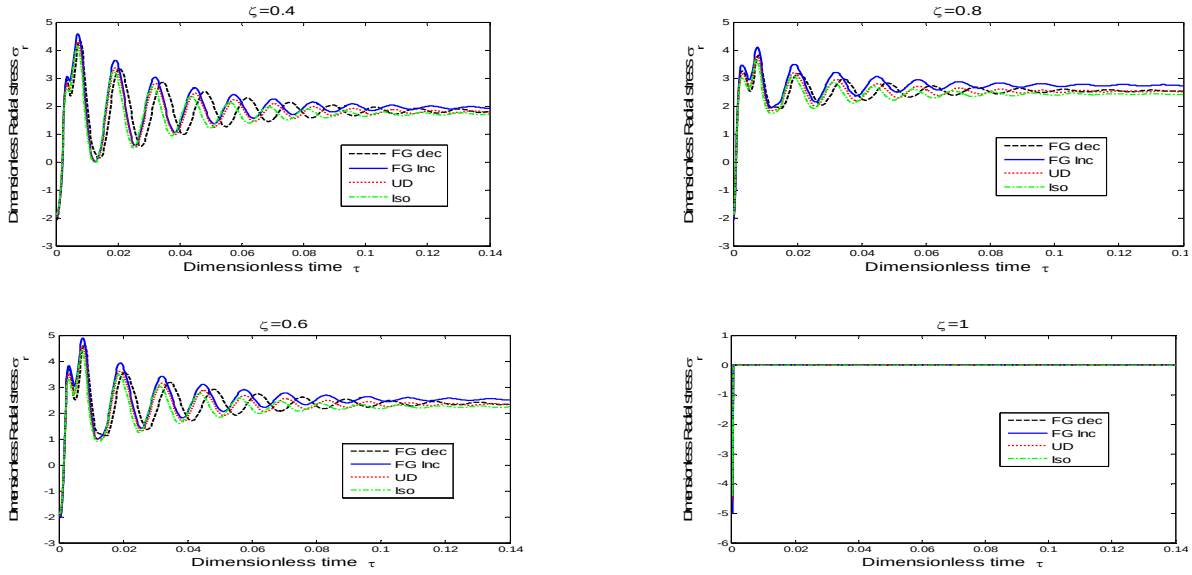

Fig. 2
Distribution of dimensionless radial stress σ_r versus dimensionless time τ for CNT reinforced cylinder for different layouts and dimensionless radius.

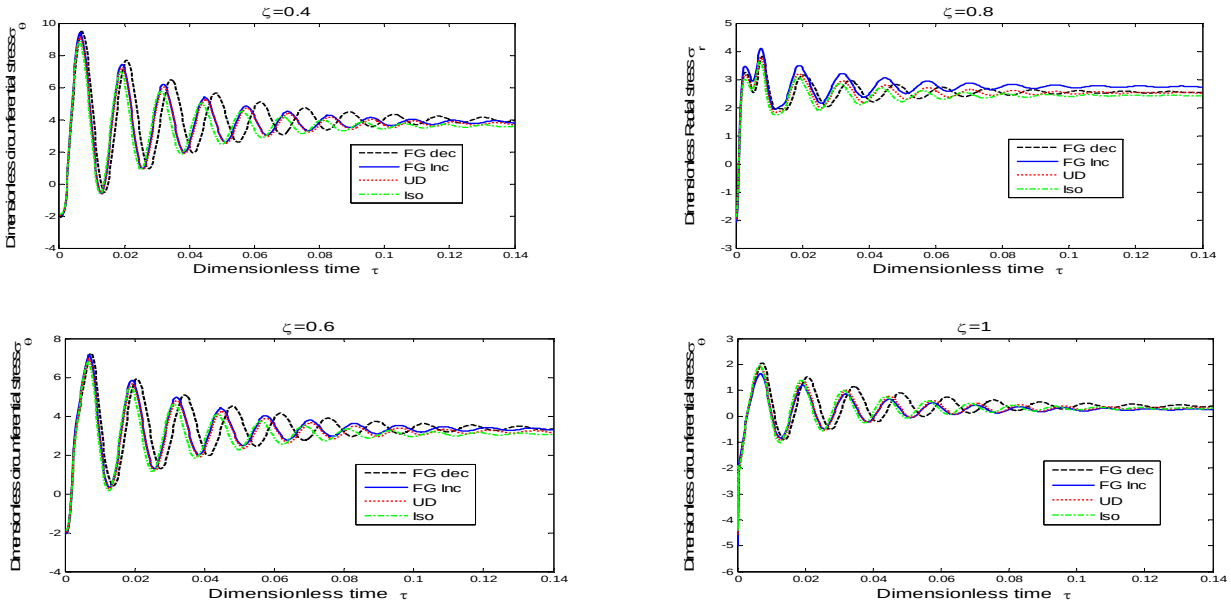

Fig. 3
Distribution of dimensionless circumferential stress σ_θ versus dimensionless time τ for CNT reinforced cylinder for different layouts and dimensionless radius**.**

Fig.4 illustrates the perturbation of magnetic field vector (h_z) versus dimensionless time (τ) for various layouts. The amplitude of h_z decreases with increasing ζ and τ values. Moreover, perturbations of magnetic field vector reaches stability earlier for Iso conditions as compared to others. h_z's at the steady state do not change from inner to outer surface. There is no difference in maximum values of perturbation of magnetic field vector amongst layouts.

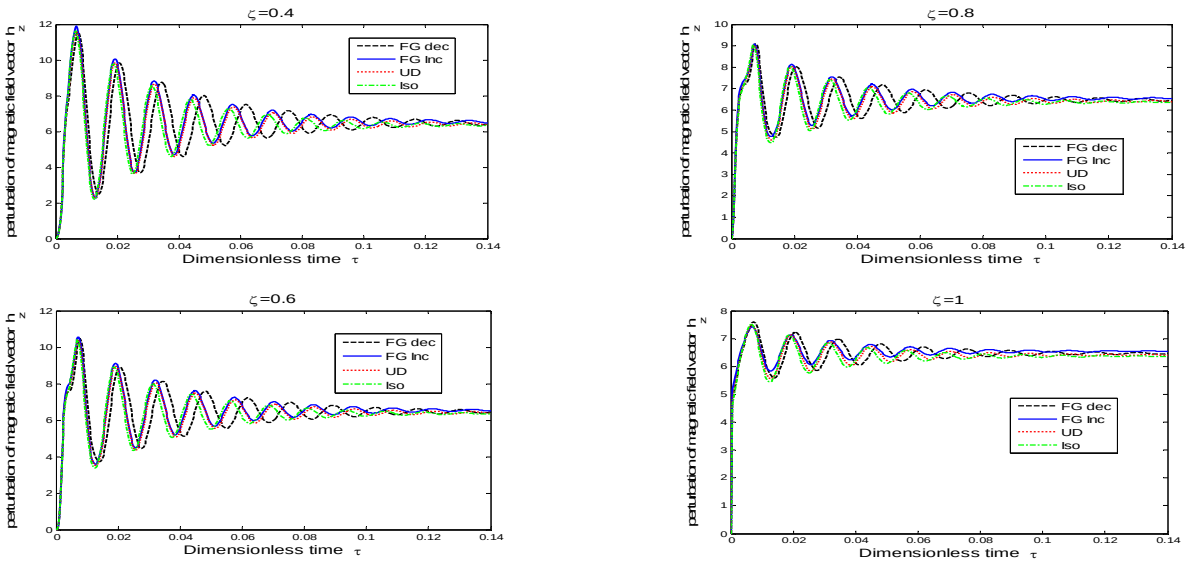

Fig. 4

Distribution of dimensionless perturbation of magnetic field vector h_z versus dimensionless time τ with CNT reinforced cylinder for different layouts and dimensionless radius.

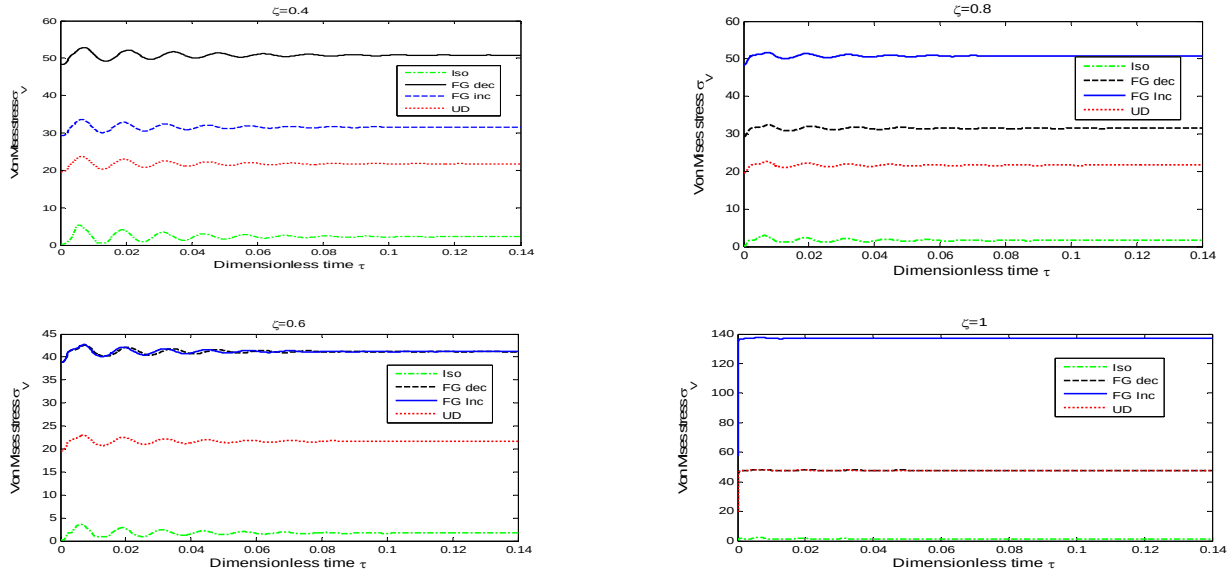

Fig. 5

Distribution of dimensionless Von Mises stress σ_v versus dimensionless time τ with CNT reinforced cylinder for different layouts and dimensionless radius.

Fig. 5 shows distribution of Von-Mises stress (σ_V) versus dimensionless time (τ) for different layouts. With increasing ζ and τ, Von-Mises stress do not change considerably for Iso condition and UD layout. However, σ_V increases for FG Inc layout and decreases for FG dec layout from inner to outer surface. It means Iso condition and UD layout offer the best design condition. It is interesting to note that Von-Mises stresses are larger than radial and circumferential stresses indicating that the axial stress has an important role in design.

4 CONCLUSIONS

In this article, magneto-thermo-elastic behavior of thick-walled cylinder made from polystyrene reinforced with FG SWCNTs in radial direction subjected to transient temperature place in a uniform magnetic field was investigated. Using Mori-Tanaka method, the constitutive equations of polymeric cylinder reinforced with CNTs were derived.
The following conclusions may be drawn from the works presented in this study:
1. Amplitude of dimensionless radial, circumferential, Von-Mises stresses and perubration magnetic field vector decrease for any layout with increase in dimensionless time and radius.
2. Steady state value of dimensionless radial stress increase for any layout from inner to middle surface; while, it decreases from middle to outer surface. Also, steady state value of dimensionless circumferential stress decreases from inner to outer surface; while it does not vary for perturbation magnetic field vector.
3. Dimensionless radial, circumferential stresses and perturbations of magnetic field vector stabilizes earlier in isotropic condition (Iso) compare to others; while Von-Mises stress values do not change for any layout.
4. Maximum radial and minimum circumferential stress value takes place for FG Inc and FG dec, respectively.
5. After Iso condition, UD lay out is recommended for optimum design of nano composite thick-walled cylindrical vessels as minimum Von-Mises stress toward the FG structures.

APPENDIX

$$\begin{Bmatrix}\sigma_r\\ \sigma_z\\ \sigma_\theta\\ \sigma_{\theta z}\\ \sigma_{zr}\\ \sigma_{r\theta}\end{Bmatrix}=\begin{bmatrix}k+m & l & k-m & 0 & 0 & 0\\ l & n & l & 0 & 0 & 0\\ k-m & l & k+m & 0 & 0 & 0\\ 0 & 0 & 0 & p & 0 & 0\\ 0 & 0 & 0 & 0 & m & 0\\ 0 & 0 & 0 & 0 & 0 & p\end{bmatrix}\begin{Bmatrix}\varepsilon_r\\ \varepsilon_z\\ \varepsilon_\theta\\ 2\gamma_{\theta z}\\ 2\gamma_{zr}\\ 2\gamma_{r\theta}\end{Bmatrix}$$

$$k=\frac{E_m\left\{E_m c_m+2k_r(1+\nu_m)[1+c_r(1-2\nu_m)]\right\}}{2(1+\nu_m)[E_m(1+c_r-2\nu_m)+2c_m k_r(1-\nu_m-2\nu_m{}^2)]}$$

$$l=\frac{E_m\left\{c_m\nu_m[E_m+2k_r(1+\nu_m)]+2c_r l_r(1-\nu_m{}^2)\right\}}{(1+\nu_m)[2c_m k_r(1-\nu_m-2\nu_m{}^2)+E_m(1+c_r-2\nu_m)]}$$

$$p=\frac{E_m[E_m c_m+2(1+c_r)p_r(1+\nu_m)]}{2(1+\nu_m)[E_m(1+c_r)+2c_m p_r(1+\nu_m)]}$$

$$m=\frac{E_m[E_m c_m+2m_r(1+\nu_m)(3+c_r-4\nu_m)]}{2(1+\nu_m)\{E_m[c_m+4c_r(1-\nu_m)]+2c_m m_r(3-\nu_m-\nu_m{}^2)\}}$$

$$n=\frac{E_m{}^2 c_m(1+c_r-c_m\nu_m)+c_m c_r(k_r n_r-l_r{}^2)(1+\nu_m)^2(1-2\nu_m)}{(1+\nu_m)\{2c_m k_r(1-\nu_m-2\nu_m{}^2)+E_m(1+c_r-2\nu_m)\}}+\frac{E_m[2c_m{}^2 k_r(1-\nu_m)+c_r n_r(1-2\nu_m+c_r)-4c_m l_r\nu_m)]}{2c_m k_r(1-\nu_m-2\nu_m{}^2)+E_m(1-2\nu_m+c_r)}$$

REFERENCES

[1] Lau K.T., Hui D., 2002, The revolutionary creation of new advanced materials–carbon nanotube composites, *Composite Part B: Engineering* **33**: 263-277.

[2] Lau K.T., Gu C., Gao G.H., Ling H.Y., Reid S.R., 2004, Stretching process of single-and multi walled carbon nanotubes for nano composite applications, *Carbon* **42**: 426-428.

[3] Esawi A.M.K., Farag M.M., 2007, Carbon nanotube reinforced composites: potential and current challenges, *Materials and Design* **28**: 2394-2401.

[4] Qian D., Dickey E.C., Andrews R.., Rantell T., 2000, Load transfer and deformation mechanisms in carbon nanotube-polystyrene composites, *Applied Physics Letters* **76**: 2868-2870 .

[5] Fidelus J.D., Wiesel E., Gojny F.H., Schulte K., Wagner H.D., 2005,Thermo-mechanical properties of randomly oriented Carbon/epoxy nano composites, *Composite Part A: Applied Science and Manufacturing* **36**: 1555-1561 .

[6] Ghorbanpour Arani A., Maghamikia S.H., Mohammadimehr M., Arefmanesh A., 2011, Buckling analysis of laminated composite rectangular plates reinforced by SWCNTs using analytical and finite element methods, *Journal of Mechanical Science and Technology* **25**: 809-820.

[7] Shen H.S., 2009, Nonlinear bending of functionally graded carbon nanotube-reinforced composite plates in thermal environments, *Composite Structures* **91**: 9-19.

[8] Ke L.L., Yang J., Kitipornchai S., 2010, Nonlinear free vibration of functionally graded carbon nanotube-reinforced composite beams, *Composite Structures* **92**: 676-683.

[9] Shen H.S., Zhang C.H., 2010, Thermal buckling and postbuckling behavior of functionally graded carbon nanotube-reinforced composite plates, *Materials and Design* **31**: 3403-3411.

[10] Ding H.J., Wang H.M., Chen W.Q., 2001, A theoretical solution of cylindrically isotropic cylindrical tube for axisym metric plane strain dynamic thermoelastic problem, *Acta. Mechanica Solida Sinica*. **14**: 357-363.

[11] Shi D.L., Feng X.Q., Huang Y.Y., Hwang K.C., Gao H., 2004,The effect of nanotube waviness and agglomeration on the elastic property of carbon nanotube-reinforced composites, *ASME Journal of Engineering Materials and Technol*ogy **126**: 250-257.

[12] *Polymer Data Hand Book*, 1999, Oxford University Press, Oxford, 828-837.

[13] Hetnarski R.B., Eslami M.R., 2009, *Thermal Stresses-Advanced Theory and Applications,* Springer.

[14] Nan C.W., Shi Z., Lin Y., 2003, A simple model for thermal conductivity of carbon nanotube-based composites, *Chemical Physics Letters* **375**: 666-669.

[15] Peters J.E., Papavassiliou D.E., Grady B.P., 2008, Unique thermal conductivity behavior of single-walled carbon nanotube-polystyrene composites, *Macromolecule* **41**: 7274-7277.

[16] Bi K., Chen Y., Yang J., Wang Y., Chen M., 2006, Molecular dynamics simulation of thermal conductivity of single-walled carbon nanotubes, *Physics Letters A* **350**: 150-153.

[17] Dai H.L., Wang X., 2006, The dynamic response and perturbation of magnetic field vector of orthotropic cylinders under various shock loads, *International Journal of Pressure Vessels and Piping* **83**: 55-62.

[18] Lehtinen P.O., Foster A.S., Ayuela A., Vehvilainen T.T., Nieminen R.M., 2004, Structure and magnetic properties of adatoms on carbon nanotubes, *Physical Review B* **69**: 155422.

[19] Kordkheili S.A.H., Naghdabadi R., 2007, Thermoelastic analysis of a functionally graded rotating disk, *Composite Structures* **79**: 508-516.